Structure, Vol. 12, 669–676, April, 2004, ©2004 Elsevier Science Ltd. All rights reserved. DOI 10.1016/j.str.2004.03.006

A Docking Approach to the Study of Copper Trafficking Proteins: Interaction between Metallochaperones and Soluble Domains of Copper ATPases

Fabio Arnesano,[1] Lucia Banci,[1] Ivano Bertini,[1,*] and Alexandre M.J.J. Bonvin[2]
[1]Magnetic Resonance Center CERM and
Department of Chemistry
University of Florence
Via Luigi Sacconi 6
50019, Sesto Fiorentino
Florence
Italy
[2]Department of NMR Spectroscopy
Bijvoet Center for Biomolecular Research
Utrecht University
3584CH, Utrecht
The Netherlands

Summary

A structural model of the transient complex between the yeast copper chaperone Atx1 and the first soluble domain of the copper transporting ATPase Ccc2 was obtained with HADDOCK, combining NMR chemical shift mapping information with in silico docking. These two proteins are involved in copper trafficking in yeast cells. Calculations were performed starting with the copper ion either bound to Atx1 or to Ccc2 and using the experimental structures of the copper-loaded and apo forms of each protein. The copper binding motifs of the two proteins are found in close proximity. Copper tends to move from Atx1 to Ccc2, consistent with the physiological direction of transfer, with concomitant structural rearrangements, in agreement with experimental observations. The interaction is mainly of an electrostatic nature with hydrogen bonds stabilizing the complex. The structural data are relevant for a number of proteins homologous to Atx1 and Ccc2 and conserved from bacteria to humans.

Introduction

Most proteins achieve their function by interacting with other proteins and forming an active complex. Protein-protein interactions are at the basis of any biological process, as each interaction represents an essential step within a cellular pathway. The interactions between two or more proteins often are highly specific processes, which belong to a series of concatenated cellular events. Therefore, a single defective complex formation may alter cell metabolism and regulation, thus causing a disease state.

A deep understanding of mechanisms of molecular recognition and interaction can only be obtained through elucidation of the three-dimensional structure of protein complexes. However, the number of structures of complexes available in the Protein Data Bank (PDB) is still very low and mostly limited to stable complexes. The experimental structure determination of transient complexes, like those formed by electron-transfer or metal-transport systems, often requires the use of techniques, like site-directed mutagenesis or cross-linking, for the stabilization of an intermediate state. An alternative approach to the study of protein complexes is provided by in silico methods, which are particularly useful in the case of transient complexes.

In the present work, an information-driven docking approach has been applied to the case of the interaction between two proteins involved in copper transport, which represents an essential step in a copper trafficking pathway. Copper proteins are involved in vital processes such as respiration, iron transport, oxidative stress protection, blood clotting, and pigmentation (Linder, 1991). On the other hand, because of its redox activity, copper would be highly toxic even at low concentrations. Therefore, free intracellular copper is absent, and its concentrations need to be regulated within very narrow limits (Rae et al., 1999). Disturbed copper homeostasis has recently been implicated in disease states or pathophysiological conditions (Sayre et al., 1999; Bush, 2000; Strausak et al., 2001).

Copper, like other metal ions, needs to be accompanied by proteins called metallochaperones, responsible for its distribution inside the cytoplasm (O'Halloran and Culotta, 2000; Rosenzweig, 2001). Thermodynamic and kinetic considerations suggest that copper trafficking proteins overcome the extraordinary copper chelation capacity of the eukaryotic cytoplasm by catalyzing the rate of copper transfer between physiological partners. In this sense, metallochaperones work like enzymes, carefully tailoring energetic barriers along specific reaction pathways but not others.

In the baker's yeast, *Saccharomyces cerevisiae*, the copper chaperone Atx1 delivers Cu(I) to the soluble copper domains of Ccc2, an ATPase located in the trans-Golgi network (Lin et al., 1997; Pufahl et al., 1997), which then transfers copper to a cuproenzyme (Yuan et al., 1997). It has been shown that this occurs in a direct and reversible manner (Huffman and O'Halloran, 2000). The thermodynamic gradient for metal transfer is shallow ($K_{eq} = 1.5$), establishing that transfer of copper from Cu(I)-Atx1 to Ccc2 is not based on a higher copper affinity of the target domain (Huffman and O'Halloran, 2000). Instead, Atx1 protects Cu(I) from nonspecific reactions (Pufahl et al., 1997) and allows rapid metal transfer to its partner ($k_{ex} > 10^3\ s^{-1}$) (Huffman and O'Halloran, 2000; Arnesano et al., 2001a). This underscores the importance of understanding the molecular aspects related to the protein-protein recognition process, which are linked to the mechanism of metal transfer.

Solution structures of the native Cu(I)-bound and the reduced apo forms of both yeast Atx1 (72 amino acids) (Arnesano et al., 2001b) and the first soluble domain of yeast Ccc2 (Ccc2a hereafter) (72 amino acids) (Banci et al., 2001) have been solved. These structures share a classical "ferredoxin-like" β1-α1-β2-β3-α2-β4 folding (Hubbard et al., 1997) where the secondary structure

*Correspondence: bertini@cerm.unifi.it

Table 1. List of Active and Passive Residues Used in the Definition of the Ambiguous Interaction Restraints for Docking of Atx1 and Ccc2a, and Flexible Segments

Atx1	
Active residues[a]	V12, T14, C15, S16, G17, G20, N23, K24, K28, K61, K62, T63, G64
Passive residues[b]	A21, V25, T27, E30, P31, I38, L40, F55, E58, K59, K65, E66, R68
Flexible segments	10–33, 36–42, and 53–70
Ccc2	
Active residues[a]	H9, G10, C13, A15, N18, T19, Q23, C62, G63, D65
Passive residues[b]	S14, C16, T22, A26, L37, N40, E60, D61, F64, E67
Flexible segments	7–28, 35–42, and 58–69

[a] The active residues correspond to the residues having a significant NMR chemical shift perturbation during the NMR titration experiments and that are highly solvent accessible.
[b] The passive residues correspond to all surface neighbors of the active residues that are solvent accessible.

elements, four β strands and two α helices, are connected by loop regions. The copper binding motifs CxxC are located on a solvent-exposed region encompassing the first loop and the beginning of the first α helix (Rosenzweig et al., 1999; Arnesano et al., 2001b). Copper is coordinated by the two cysteines of a CxxC motif, but it expands its coordination sphere to three-coordination by binding an exogenous ligand. It has been proposed that copper exchange between Atx1 and Ccc2 occurs through a series of copper bridged intermediates (Pufahl et al., 1997).

The *h*igh *a*mbiguity *d*riven protein-protein *dock*ing approach HADDOCK (Dominguez et al., 2003) has been applied to the case of the Atx1:Ccc2a complex, taking advantage of the available NMR titration data (Arnesano et al., 2001a). The refined model of the complex provides a valid structural basis to discuss mechanistic implications of copper exchange between a metallochaperone and its partner protein.

Results

HADDOCK Calculations

The amino acids involved in the interaction between Atx1 and Ccc2a, and therefore constituting the protein-protein interface, were detected by NMR through $^{1}H/^{15}N$ chemical shift changes occurring in both proteins when titrated with the partner (Arnesano et al., 2001a). These residues are located in loops 1 and 5, helix α1, and the C-terminal part of helix α2 in both proteins. They were used to generate ambiguous interaction restraints (AIRs) as described in the Experimental Procedures (Table 1). HADDOCK was used for the docking calculations using as input the average minimized NMR structures of the two protein partners in different metalation states. The structure of Cu(I) and apo forms of both Atx1 (Arnesano et al., 2001b) and Ccc2a (Banci et al., 2001) were solved by NMR; therefore, we performed two different runs either starting from the copper ion bound to the metallochaperone Atx1 or to the domain Ccc2a of the ATPase, as detailed below:

(A) Cu(I) bound to Atx1, using as input the average minimized structure of Cu(I)-Atx1 (PDB ID 1FD8) and apoCcc2a (1FVQ);
(B) Cu(I) bound to Ccc2a, using as input the average minimized structure of apoAtx1 (PDB ID 1FES) and Cu(I)-Ccc2a (1FVS).

The copper ion was explicitly included in the docking calculations (see Experimental Procedures).

Figure 1 shows a plot of the intermolecular energy, E_{inter} (sum of intermolecular van der Waals, electrostatic, and AIR energy terms), for the 100 refined complex structures after water refinement as a function of their backbone rmsd from the lowest energy structure. After analysis, two clusters were obtained in each run (A and B). Their statistical results are summarized in Table 2.

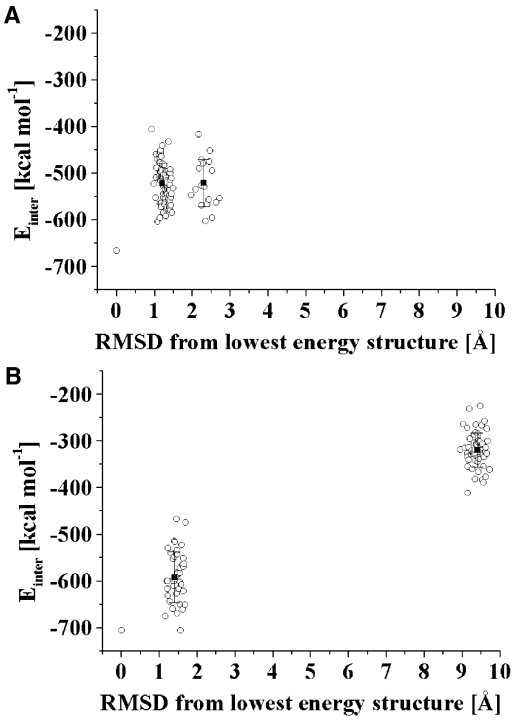

Figure 1. Intermolecular Energies versus Backbone Rmsd at the Interface from the Lowest Energy Structure for the Atx1:Ccc2a Complex

The structural ensembles obtained after water refinement correspond to (A) Cu(I)-Atx1 and apoCcc2a, and (B) apoAtx1 and Cu(I)-Ccc2a. The values for single conformations (open circles) and cluster averages (closed squares) are shown. The intermolecular energy corresponds to the sum of AIR, van der Waals, and electrostatic energy terms. The nonbonded energies were calculated with the OPLS parameters (Jorgensen and Tirado-Rives, 1998) using a 8.5 Å cut-off. The clustering was based on the pairwise backbone rmsd using a 1.75 Å cut-off.

Table 2. Statistical Analysis of HADDOCK Results for the Two Different Runs after Clustering of Solutions for the Atx1:Ccc2a Complex

	Rmsd (Å)[a]	Rmsd min (Å)[b]	Number of Structures	E_{inter} (kcal mol^{-1})	E_{vdw}[c] (kcal mol^{-1})	E_{elec}[c] (kcal mol^{-1})	E_{AIR} (kcal mol^{-1})	Number of AIR Violations (>0.3 Å)	Buried Surface Area (Å^2)
A									
Cluster 1	1.2 ± 0.2	1.2 ± 0.2	82	−522 ± 43	−45	−479.5	2.47	2.4 ± 0.7	1259 ± 55
Cluster 2	1.3 ± 0.4	2.3 ± 0.2	17	−521 ± 51	−54	−469	1.36	1.3 ± 1.0	1302 ± 71
B									
Cluster 1	1.4 ± 0.2	1.4 ± 0.2	42	−592 ± 55	−49	−544	0.65	1.0 ± 0.3	1310 ± 60
Cluster 2	1.3 ± 0.2	9.4 ± 0.2	54	−319 ± 37	−40	−282	1.85	2.0 ± 1.2	1123 ± 61

Clusters are sorted according to average intermolecular energy.
[a] Average rmsd and standard deviation from the lowest energy structure of the cluster.
[b] Average rmsd and standard deviation from the lowest energy structure of all calculated structures.
[c] The nonbonded energies were calculated with the OPLS parameters (Jorgensen and Tirado-Rives, 1998) using an 8.5 Å cut-off.

The clusters are ranked according to their average intermolecular energies. In both cases, cluster 1 has the lowest average value of intermolecular energies. The lowest energy cluster (cluster 1) in each run also contains the lowest energy structure. For all the clusters, E_{elec} represents the major energy contribution to E_{inter}, being about one order of magnitude larger than E_{vdw}. E_{AIR} is instead very small, with values between 0.65 and 2.47 kcal mol^{-1}, consistent with a very low number of AIR violations per structure. Average values of buried surface areas for the various clusters range from 1123 to 1302 Å^2.

Clusters 1 and 2 of run A (see Table 2) have very similar average E_{inter}. However, the first cluster contains a larger number of structures as well as the overall lowest energy structure. The average rmsd values to the lowest energy structure are 1.2 ± 0.2 and 2.3 ± 0.2 Å for cluster 1 and 2, respectively, indicating that the conformations of the two clusters are not remarkably different.

Run B produces two clusters containing a comparable number of structures; however, the structures of cluster 2 have higher intermolecular energies, with an average of −319 ± 37 kcal mol^{-1} compared to a E_{inter} value of −592 ± 55 kcal mol^{-1} for cluster 1. The average rmsd to the overall lowest energy structure is 1.4 ± 0.2 Å and 9.4 ± 0.2 Å for cluster 1 and 2, respectively, indicating very different conformations for the two clusters.

The rmsd values to the average of the ten best structures of the lowest energy clusters are given in Table 3. Generally, the rmsd of backbone atoms of residues at the interface is higher than the rmsd of all backbone atoms of both partners, which indicates a local rearrangement of the protein surface during the docking process to adapt to the partner. In all cases, larger rmsd values are found for the Atx1 moiety of the complex. Figures 2A and 2B show a representation of two different structural ensembles where the radius of the tube is proportional to the backbone rmsd per residue.

The backbone rmsd value between the average structure of run A (copper ion bound to Atx1) and of run B (copper bound to Ccc2a) is 2.07 Å. When the two ensembles, each containing the ten best structures of A and B, are merged, the rmsd to the average structure is 1.3 Å, which gives an indication of the degree of convergence of runs A and B to a unique solution.

Description of the Calculated Structures of the Atx1:Ccc2a Complex

Atx1 and Ccc2a in the complex maintain their global fold. In all the structures, helix α1 of one protein is nearly orthogonal to helix α2 of the partner and in contact with loop 5. The copper binding CxxC motifs of Atx1 and Ccc2a are juxtaposed in the complex. The average intermolecular distances between pairs of sulfur atoms are reported in Table 4. Their values are between 4 and 6 Å for run A. Slightly higher values (7–8 Å) are found for run B. In the complex calculated starting from Cu(I)-Atx1 (run A), copper is located at a very small distance (i.e., 3.7 Å on average), being sometimes at bonding distance (<2.4 Å), from the sulfur atom of C13 of Ccc2a, as a result of the semiflexible simulated annealing in torsion angle space performed in HADDOCK. Run B gives larger distances (7–8 Å) between the copper ion, which is linked to Ccc2a, and the cysteines of apoAtx1, although in some structures distances as small as 4.5 Å are observed (Table 4).

Besides metal ion coordination, the complex is stabilized by an extended network of intermolecular hydrogen bonds and salt bridges (see Supplemental Material at http://www.structure.org/cgi/content/full/12/4/669/

Table 3. Average Rmsd Values from the Average Structure Calculated over the Ensemble of the Ten Best Structures of the Lowest Intermolecular Energy Cluster, Cluster 1, for the Two HADDOCK Runs

	Rmsd (Å)	
Calculations	A	B
Rmsd of backbone atoms of Atx1:Ccc2a complex	0.74 ± 0.21	0.79 ± 0.26
Rmsd of backbone atoms of Atx1	0.79 ± 0.23	0.84 ± 0.30
Rmsd of backbone atoms of Ccc2a	0.68 ± 0.18	0.75 ± 0.22
Rmsd of backbone atoms on interface	0.73 ± 0.20	0.87 ± 0.29

Structures are superimposed on the backbone atoms of the flexible interface.

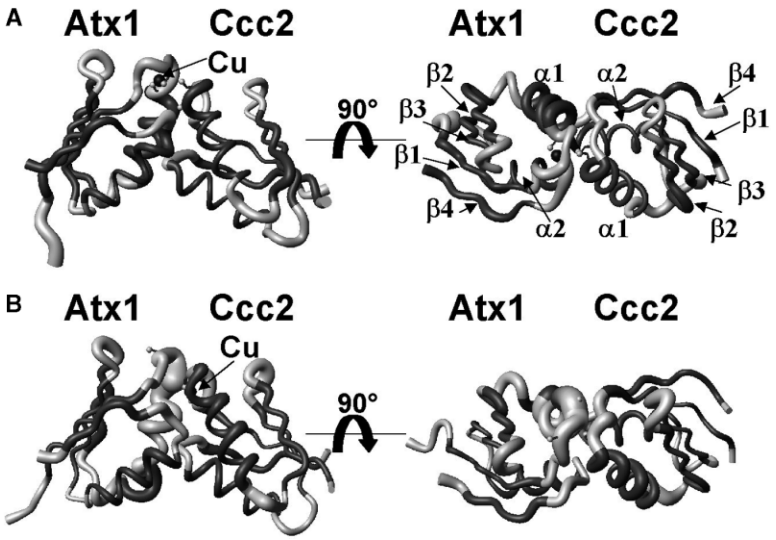

Figure 2. Ensemble of the Ten Best Structures of the Lowest Intermolecular Energy Cluster Generated by HADDOCK

The structural ensembles of the complex are obtained from (A) Cu(I)-Atx1 and apoCcc2a, and (B) apoAtx1 and Cu(I)-Ccc2a. On the right side, the structures are viewed 90° from the orientation of those on the left side. The radius of the tube is proportional to the backbone rmsd of each residue. Secondary structure elements are indicated in dark gray. The Cu(I) ion is shown as a black sphere. The sulfur atoms of copper binding cysteines are represented as light gray spheres. The figure was generated with MOLMOL (Koradi et al., 1996).

DC1) involving both charged and polar amino acids at the interface between the two proteins, as expected on the basis of a large contribution of E_{elec} to the overall intermolecular energy E_{inter} (Table 2). The identity and the number of less conserved hydrogen bonds may vary from one run to another, but some electrostatic interactions are consistently found in all the calculations. These interactions occur between K24 of Atx1 and D65 of Ccc2a, K28 of Atx1 and E60 of Ccc2a, and K59 and K62 of Atx1 and D61 of Ccc2a (Figure 3). These interactions may optimize the relative orientation of the two proteins to allow a close contact between the two metal binding regions.

Given the mainly electrostatic nature of the interaction between Atx1 and Ccc2a, conserved intermolecular hydrophobic contacts are few, the more frequent occurring between A21 of Atx1 and F64 of Ccc2a, and V25 of Atx1 and G63 of Ccc2a. Some less conserved contacts involve the metal binding cysteines; e.g., C15 of Atx1 can interact with A15 of Ccc2a, and C13 of Ccc2a with S16 and G17 of Atx1. Ccc2a contains four additional cysteines, i.e., C33, C42, C62, and C66. C62 is found at the interface and is in contact with K62 of Atx1.

Comparison with Experimental Structures

The Cu(I)-Atx1 and apoCcc2a structures do not experience sizable changes upon complex formation in run A.

Table 4. Average Interatomic Distances between the Sulfur Atoms of Copper Binding Cysteines of Atx1 and Ccc2a and between the Sulfur Atoms and the Copper Ion Calculated over the Ensemble of the Ten Best Structures of Cluster 1 for the Two HADDOCK Runs

			Interatomic Distance (Å)	
Atx1	Ccc2a	Cu	A	B
Cys 15 Sγ	Cys 13 Sγ		4.2 ± 0.9	8.1 ± 1.3
Cys 15 Sγ	Cys 16 Sγ		5.2 ± 1.5	8.0 ± 0.8
Cys 18 Sγ	Cys 13 Sγ		5.0 ± 1.5	7.0 ± 2.0
Cys 18 Sγ	Cys 16 Sγ		6.2 ± 2.0	8.1 ± 1.5
Cys 15 Sγ		Cu	2.1 ± 0.1	7.9 ± 1.5
Cys 18 Sγ		Cu	2.0 ± 0.1	7.0 ± 2.5
	Cys 13 Sγ	Cu	3.7 ± 1.5	2.2 ± 0.2
	Cys 16 Sγ	Cu	6.1 ± 1.5	2.2 ± 0.2

Indeed, the backbone rmsd between the experimental structures used as input in run A and the average structure of the complex is 0.99 Å for the Atx1 moiety and 0.68 Å for Ccc2a, indicating a substantially similar structure before and after docking. In Atx1 some meaningful changes are observed: (1) a one-turn shortening at the N terminus of helix α1 and (2) a slight shift of helix α2 and loop 5 of Atx1. In addition, some structures show a movement of the side chain of C18 of Atx1 from inside to outside due to an ~90° rotation around the Cα-Cβ bond of the cysteine, which is located at the N terminus of helix α1. As a consequence, in these structures the copper atom moves toward the metal binding cysteines of Ccc2a (Figure 4A). This determines a relatively large rmsd (~3 Å) of the copper atom within the structural ensemble of run A. In the NMR structure of Cu(I)-Atx1, the Nζ atom of the side chain of K65, which is located in loop 5, is found very close to the copper ion [Cu(I)-Nζ (K65) = 5 ± 1 Å]. After docking, the side chain of K65 moves farther from Cu(I) and forms a hydrogen bond either with the side chain of N18 of Ccc2a or the backbone oxygen of A15 of Ccc2a. In the solution structure of apoAtx1, the side chain of K65 is highly disordered (Arnesano et al., 2001b).

The solution structure of Atx1 in the presence of one equivalent of Ccc2a (adduct-Atx1, hereafter) has been experimentally determined (Arnesano et al., 2001a). This structure has intermediate features between those of the free Cu(I)-bound and apo states of Atx1. The backbone rmsd values between Cu(I)-Atx1 and adduct-Atx1 and between apoAtx1 and adduct-Atx1 are 1.27 and 1.45 Å, respectively. For comparison, the rmsd between Cu(I)- and apoAtx1 is 1.53 Å. Structural variations within these structures occur in the vicinity of the metal binding site (Arnesano et al., 2001a, 2001b). Apo and Cu(I)-Ccc2 structures are instead very similar (Banci et al., 2001).

The lowest pairwise backbone rmsd between two structures belonging to different ensembles is 1.7 Å, and it is found between structure 4 of run A and structure 3 of run B. In structure 4 of run A, the copper ion is the most protruded toward the Ccc2a protein and at bonding distance from the N-terminal Cys of the CxxC motif of Ccc2a. Notably, the Atx1 protein of structure 4 of run A is also the closest to the NMR structure of

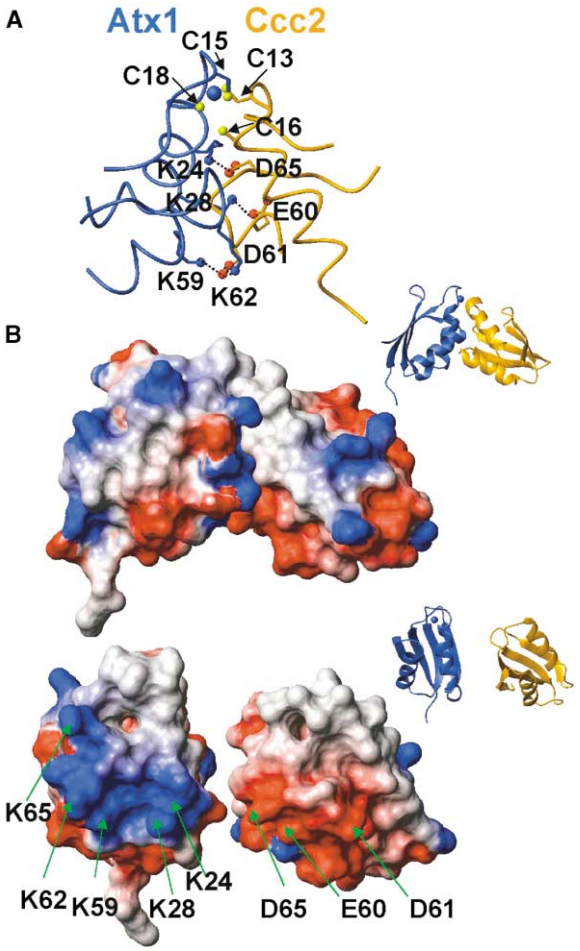

Figure 3. Hydrogen Bonding Interactions and Electrostatic Surface Potential of the Atx1:Ccc2a Complex

(A) Conserved hydrogen bonding interactions in the structures of the complex generated by HADDOCK. Atx1 is shown in blue, Ccc2a is shown in orange, and the Cu(I) ion is represented as a blue sphere. Residues involved in hydrogen bonding interactions and the copper binding cysteines are indicated.

(B) Electrostatic surface potential (left side) and ribbon representation (right side) of the complex. The positively charged, negatively charged, and neutral amino acids are represented in blue, red, and white, respectively. In the bottom view, the molecules are rotated by 90° to show the interaction surfaces.

adduct-Atx1, with a backbone rmsd value of 1.2 Å between the two structures.

The structures with the lowest intermolecular energies in test HADDOCK calculations (Dominguez et al., 2003) were the closest to the experimental structure of the respective complexes (within 2.0 Å backbone rmsd). In the absence of experimental structural data on the Atx1:Ccc2a complex, the HADDOCK structures of the complex can be compared with the X-ray structure of Hah1, the human homolog of Atx1, which crystallizes as a homodimer (Wernimont et al., 2000). The structure of Cu(I)-Hah1 reveals a copper ion coordinated by cysteine residues from two adjacent Hah1 molecules in a distorted tetrahedral array, with the fourth ligand weakly bound (Wernimont et al., 2000). When superimposing the ten structures of the HADDOCK ensemble generated in run A on the coordinates of Cu(I)-Hah1, an average backbone rmsd of 3.0 ± 0.2 Å is obtained for the overlapping segments. Atx1 is superimposed on one monomer of Hah1, and Ccc2a is superimposed on the other monomer, on the basis of the structure-based multiple sequence alignment of Hah1, Atx1, and Ccc2a, excluding gaps. Taking into account sequence variations between Hah1, Atx1, and Ccc2a and that Atx1:Ccc2a is a heterodimeric complex while Cu(I)-Hah1 is a homodimer, the structures can be considered remarkably similar. It has been pointed out that CxxC motifs in the Hah1 dimer are stabilized by a hydrogen bonding network in addition to the copper coordination (Wernimont et al., 2000). In particular, an intermolecular hydrogen bond between the sulfur of the N-terminal cysteine of the motif (C12) and the side chain oxygen of a conserved threonine (T11) preceding the same cysteine, on the opposite protein molecule, is observed in the Hah1 structure. In our structures, the distance between these two atoms is too large (about 8–9 Å), but a 4°–5° rotation of the Atx1 moiety with respect to Ccc2a is sufficient to form such hydrogen bond (Figure 4B).

Discussion

Mechanistically, it has been proposed that a low activation barrier for metal transfer between partners results from complementary electrostatic forces that ultimately orient the metal binding loops of Atx1 and Ccc2 for formation of copper-bridged intermediates (Huffman and O'Halloran, 2000). In addition, comparison of the Atx1 structure with the structures of homologous metallochaperones indicates that in most of the cases metal binding affects a hydrophobic patch around the metal site, possibly for tuning and optimizing the hydrophobic interactions with the ATPase domains (Banci et al., 2003). The robustness of the HADDOCK approach is demonstrated by the close proximity of the copper binding CxxC motifs in the calculated complex structures, which is not imposed by any restraint and supports a direct metal ion exchange. Indeed, the ambiguous interaction restraints, based on chemical shift perturbation data obtained from NMR titration experiments, in principle, contain no information on the relative orientation of the two partners in the complex. The discrimination between orientations comes mainly from the electrostatic and van der Waals energy terms. Atx1 possesses multiple positively charged residues on its surface (Rosenzweig et al., 1999; Arnesano et al., 2001b), while Ccc2 possesses multiple negatively charged residues (Banci et al., 2001). Most of them are strictly conserved in all the eukaryotic homologs of the yeast proteins. Mutational studies on Atx1 reveal that altering K24 and K28 to glutamates dramatically reduces the activity of Atx1, while mutations of K61 and K62 reduce function to a lesser extent (Portnoy et al., 1999). In the present docked complex, K24, K28, and K62 are involved in stable intermolecular electrostatic interactions with glutamate and aspartate residues of Ccc2a (see Figure 3), which are essential to properly orient the two molecules.

After protein-protein recognition, the copper ion is transferred from Atx1 to apoCcc2a. Comparison of the Cu(I) and apoAtx1 structures reveals that the overall folding in the two states is similar, with the exception

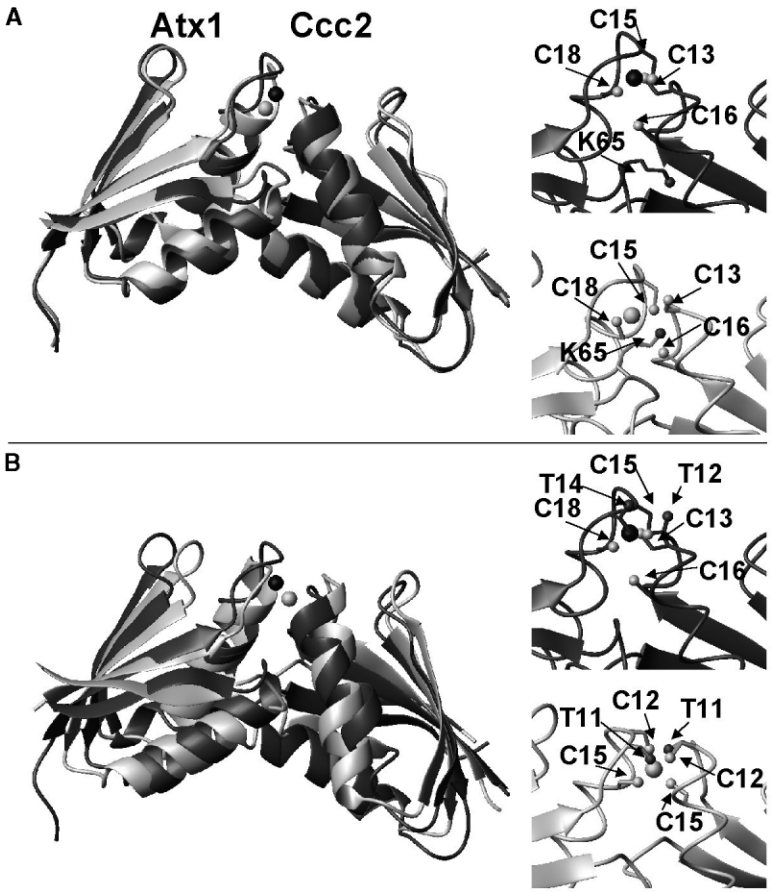

Figure 4. Comparison of the Structure of the Atx1:Ccc2a Complex with Experimental Structures

(A) Overlay of the structure of the Atx1:Ccc2a complex generated by HADDOCK and the structures of Cu(I)-Atx1 (1FD8) and apoCcc2a (1FVQ) used as input in the calculations. Atx1 and Ccc2a in the docked complex are shown in dark gray, and the Cu(I) ion is shown as a black sphere. The experimental structures of Cu(I)-Atx1 and apoCcc2a and the Cu(I) ion are shown in light gray. Details of the interaction surface of the two proteins in the complex and in the free forms are presented on the right-hand side in the same orientation as in the left side. The copper binding cysteines of Atx1 and Ccc2a and residue K65 of Atx1 are indicated.

(B) Overlay of the structure of the Atx1:Ccc2a complex generated by HADDOCK and the dimeric crystal structure of Cu(I)-Hah1 (1FEE), a human homolog of yeast Atx1. The two monomers of Hah1 and the Cu(I) ion are shown in light gray. Details of the interaction surface of the Atx1:Ccc2a complex and of the homodimerization surface of Cu(I)-Hah1 are presented on the right-hand side in the same orientation as in the left side. The cysteines of the CxxC motif of Atx1, Ccc2a, and Hah1 and the conserved threonine residue before the CxxC motif are indicated.

that helix α1 is shorter by one turn at the N terminus in the apo form (Arnesano et al., 2001b). The Cu(I) binding cysteines move from a buried site in the bound metal form to a solvent-exposed conformation on the surface of the protein after copper release. In addition, the positive charge of the side chain of K65 (loop 5) of Atx1 is no longer attracted to the protonated cysteines when copper is released. In fact, in apoAtx1, K65 moves away from the metal site, favored by a concomitant translation of helix α2 and loop 5 (Arnesano et al., 2001b). Mutation of K65 of Atx1 to glutamate abrogates the function of this protein (Portnoy et al., 1999), thus highlighting its important role in metallochaperone function. In contrast, Ccc2a contains a phenylalanine residue at this position (Arnesano et al., 2002).

All the changes associated with Cu(I) release from Atx1 are observed in most conformers of HADDOCK calculations, where residues at the interface are free to move (see Figure 4A). In Cu(I)-Atx1, residues 17–20, constituting the first turn of helix α1, determine an attractive interaction between the field generated by the helix and the cysteine thiolates, whereas they are not in a helical structure in apoAtx1, as well as in many conformers of the docked complex. K65, which is found very close to copper in the Cu(I)-Atx1 structure and is disordered in apoAtx1, tends to form intermolecular hydrogen bonds with Ccc2a in the docked complex. The peptide dipoles of the first turn at the N terminus of helix α1 and the positive charge of the side chain of Lys 65 create a more positive potential which stabilizes the negative charge of the Cu(I) bis thiolate center in Cu(I)-Atx1. Therefore, they may have a role in the electrostatic control of metal ion coordination.

Cyanobacteria have a peculiar cellular organization that involves intracellular compartments called thylakoids containing cytochrome c oxidase and plastocyanin, both proteins requiring copper to function. In these bacteria, two copper transporting ATPases are present, CtaA and PacS (Tottey et al., 2002). The former is located on the external cellular membrane and is involved in copper uptake, while the latter is on the thylakoid membrane and transports copper inside this compartment for its delivery to copper-requiring proteins (Tottey et al., 2001). Copper is shuttled between these two ATPases by a small soluble protein, homologous to yeast Atx1, which is able to interact with the soluble copper binding domains of both ATPases (Tottey et al., 2002). Interestingly, this copper chaperone possesses a histidine residue on loop 5 in the corresponding position of K65 in yeast Atx1. The imidazole ring of the histidine is proposed to provide a putative third copper ligand and to influence the direction of metal transfer in the interaction of the chaperone with the N-terminal domains of the two ATPases, PacS and CtaA (Cavet et al., 2003). An outward movement of the histidine, analogous to that of K65, would displace this predicted third copper ligand and promote copper release to PacS. Conversely, entry of the histidine into a shared binding site with CtaA would favor release to Atx1.

In yeast, structural changes between Cu(I)- and

apoAtx1 are also accompanied by an increase in the number of conformational exchange processes in a millisecond to microsecond timescale (Arnesano et al., 2001a). Notably, this mobility involves Atx1 residues that change the most in chemical shift perturbation analysis (Arnesano et al., 2001a) and that are located at the interface of the present docked complex. Thus, mobility in this region of apoAtx1 could favor complex dissociation of the two proteins after copper release. On the other hand, the difference in the dynamic behavior observed in the Cu(I)-loaded and apoCcc2a is less pronounced, according to the fact that the two forms of the protein are structurally very similar. Therefore, apoCcc2 is preorganized to some extent to receive the copper ion, and indeed, HADDOCK calculations show that sulfur atoms of copper binding cysteines of Ccc2a get very close in the complex to the metal ion bound to Atx1 (run A) (see Table 4). The dynamic behavior of Atx1 is therefore important for Cu(I) delivery to Ccc2 and is activated by a trigger mechanism expelling Cu(I) from the Atx1 site. In some HADDOCK conformers of run A, a rotation of the Atx1 C18 side chain primes the Cu(I) ion to bind to Ccc2a cysteines. These structures are the closest to those calculated starting from apoAtx1 and Cu(I)-Ccc2a, indicating that they represent well a copper-bridged intermediate state with Cu(I) bound by both molecules. The Atx1 moiety in these structures is more similar to the experimentally determined (Arnesano et al., 2001a) structure of Atx1 in the presence of Ccc2a. Summarizing, in the adduct copper is structurally and energetically favored to move toward its recipient protein, and thus we obtain from these calculations a very reliable model of the complex.

Docking calculations, here applied to a eukaryotic copper trafficking system, revealed the interaction mode and indicated structural changes at the basis of the metal transfer process. The calculated complex structures can contribute to identify crucial residues at the interface between the two proteins and are in agreement with data available from mutational analysis. HADDOCK calculations were performed leaving the backbone and the side chains of residues at the interface free to adapt their conformation upon complex formation. Therefore, examination of the structural ensembles also provides hints on the structural changes occurring in both protein partners before and after docking. These results are relevant for a large number of metal trafficking proteins sharing the same fold of Atx1 and Ccc2a and containing a similar consensus motif for metal binding. Among them are the human metallochaperone Hah1, a structural homolog of Atx1 that delivers Cu(I) to soluble metal binding domains of Menkes and Wilson proteins, two human ATPases homologous to yeast Ccc2 and involved in severe neurological disorders related to copper transport and homeostasis.

Experimental Procedures

Definition of AIRs

The "active" residues correspond to all residues showing a significant chemical shift perturbation ($\Delta\delta$) upon complex formation as well as a high solvent accessibility in the free form of the protein (>50% relative accessibility as calculated with NACCESS) (Dominguez et al., 2003). The threshold to define significant chemical shift perturbations was taken for each protein as the average over all the $\Delta\delta$ values plus 1 σ (standard deviation). Solvent-accessible residues whose cross-peaks in NMR spectra disappeared upon complex formation were also considered as "active." The "passive" residues correspond to the residues that show a less significant chemical shift perturbation and/or that are surface neighbors of the active residues and have a high solvent accessibility (>50%). Thirteen amino acids of Atx1 and ten amino acids of Ccc2a were used as "active" ambiguous interaction restraints (AIRs) (Table 1). By displaying these amino acids on the free form structures, we defined 13 "passive" amino acids for Atx1 and 10 for Ccc2a (Table 1). The position of the copper atom with respect to the ligand groups (C15 and C18 in Atx1; C13 and C16 in Ccc2a) was defined by including additional distance restraints of 2.3 $\pm$ 0.2 Å between the copper and the sulfur atom. This distance corresponds to the one typically used in NMR structure calculations. The use of distance restraints instead of covalent bonds for the copper atom allows somewhat more freedom in its position in the complex. These, together with the AIR restraints used for docking, are available as Supplemental Material (at http://www.structure.org/cgi/content/full/12/4/669/DC1). The force constants for the AIR restraints were set to 10 kcal mol^{-1} Å^{-2} for the rigid-body docking stage and then scaled up to a final value of 50 kcal mol^{-1} Å^{-2} during the semiflexible simulated annealing stage (see below). The effective distance r_{eff} was calculated as a sum average ($r_{eff} = [\Sigma 1/r^6]^{-1/6}$) over all individual pairwise combinations. All atoms of a residue are taken into account in the sum, since, despite the fact that the interaction is typically monitored by NMR on the backbone (H_N,N), direct intermolecular contacts are more likely to involve side chain atoms (for details, see Dominguez et al., 2003). The AIR restraint will be satisfied as soon as any one of the distances entering the sum average are within the defined cut-off distance (2 Å).

Docking Protocol

The docking calculations were performed with the standard HADDOCK protocols as described in Dominguez et al. (2003). For each run, 500 rigid-body docking solutions were first generated by energy minimization. The driving force for the docking at this stage comes mainly from the AIR restraints and from van der Waals and electrostatic energy terms once the structures are within the nonbonded cut-off (8.5 Å). The 100 best solutions according to the AIR restraint energy (as defined in Dominguez et al., 2003) were subjected to semiflexible simulated annealing in torsion angle space followed by a final refinement in explicit water (Linge et al., 2003). During the simulated annealing and the water refinement, the amino acids at the interface (side chains and backbone) are allowed to move to optimize the interface packing. The interface amino acids, which constitute the flexible segments, are defined by the active and passive amino acids used in the AIRs $\pm$ 2 sequential amino acids (Table 1). The nonbonded energies were calculated with the OPLS parameters (Jorgensen and Tirado-Rives, 1998) using a 8.5 Å cut-off. The electrostatic energy was calculated with an epsilon value of 1. While this choice might result in strong electrostatic interactions during the vacuum part of the protocol (rigid-body docking and semiflexible annealing), no deformations of the structures are expected, since a major part of them is kept rigid. The final refinement stage, during which more flexibility is introduced, is performed in the presence of explicit solvent.

Analysis

The final structures were clustered using pairwise backbone rmsd: structures were superimposed on backbone atoms of Atx1, and the rmsd was calculated on backbone atoms of both partners. A cluster was defined as an ensemble of at least four conformations displaying a pairwise rmsd smaller than 1.75 Å. Clusters were ranked according to their average interaction energies. The buried surface area was calculated by taking the difference between the sum of the solvent-accessible surface area for each partner separately and the solvent-accessible area of the complex. The solvent-accessible area was calculated using a 1.4 Å water probe radius. The ten best structures of the lowest energy cluster of each HADDOCK run were analyzed in terms of intermolecular contacts, and an average structure was calculated by superimposing the structures on the backbone atoms of the flexible segments (Table 1). Intermolecular contacts (hydrogen bonds and nonbonded contacts) were analyzed

with DIMPLOT, which is part of the LIGPLOT software (Wallace et al., 1995), using the default settings (3.9 Å heavy-atoms distance cut-off for nonbonded contacts; 2.7 Å and 3.35 Å proton-acceptor and donor-acceptor distance cut-offs, respectively, with minimum 90° angles [D-H-A, H-A-AA, D-A-AA] for hydrogen bonds) (McDonald and Thornton, 1994).

Acknowledgments

This work has been supported by the European Commission (contracts HPRI-CT-2001-50028 and QLG2-CT-2002-00988), the Italian MURST Project COFIN01, and Ente Cassa di Risparmio di Firenze. A.M.J.J.B. acknowledges financial support from a "Jonge Chemici" grant from the Netherlands Organization for Scientific Research (NWO).

Received: December 10, 2003
Revised: January 15, 2004
Accepted: January 20, 2004
Published: April 6, 2004

References

Arnesano, F., Banci, L., Bertini, I., Cantini, F., Ciofi-Baffoni, S., Huffman, D.L., and O'Halloran, T.V. (2001a). Characterization of the binding interface between the copper chaperone Atx1 and the first cytosolic domain of Ccc2 ATPase. J. Biol. Chem. *276*, 41365–41376.

Arnesano, F., Banci, L., Bertini, I., Huffman, D.L., and O'Halloran, T.V. (2001b). Solution structure of the Cu(I) and Apo forms of the yeast metallochaperone, Atx1. Biochemistry *40*, 1528–1539.

Arnesano, F., Banci, L., Bertini, I., Ciofi-Baffoni, S., Molteni, E., Huffman, D.L., and O'Halloran, T.V. (2002). Metallochaperones and metal transporting ATPases: a comparative analysis of sequences and structures. Genome Res. *12*, 255–271.

Banci, L., Bertini, I., Ciofi-Baffoni, S., Huffman, D.L., and O'Halloran, T.V. (2001). Solution structure of the yeast copper transporter domain Ccc2a in the apo and Cu(I)-loaded states. J. Biol. Chem. *276*, 8415–8426.

Banci, L., Bertini, I., and Del Conte, R. (2003). The solution structure of apo CopZ from *Bacillus subtilis*: a further analysis of the changes associated with the presence of copper. Biochemistry, in press.

Bush, A.I. (2000). Metals and neuroscience. Curr. Opin. Chem. Biol. *4*, 184–191.

Cavet, J.S., Borrelly, G.P., and Robinson, N.J. (2003). Zn, Cu and Co in cyanobacteria: selective control of metal availability. FEMS Microbiol. Rev. *27*, 165–181.

Dominguez, C., Boelens, R., and Bonvin, A.M.J.J. (2003). HADDOCK: a protein-protein docking approach based on biochemical or biophysical information. J. Am. Chem. Soc. *125*, 1731–1737.

Hubbard, T.J.P., Murzin, A.G., Brenner, S.E., and Chothia, C. (1997). A structural classification of proteins database. Nucleic Acids Res. *25*, 236–239.

Huffman, D.L., and O'Halloran, T.V. (2000). Energetics of copper trafficking between the Atx1 metallochaperone and the intracellular copper-transporter, Ccc2. J. Biol. Chem. *275*, 18611–18614.

Jorgensen, W.L., and Tirado-Rives, J. (1998). The OPLS potential function for proteins. Energy minimization for crystals of cyclic peptides and Crambin. J. Am. Chem. Soc. *110*, 1657–1666.

Koradi, R., Billeter, M., and Wüthrich, K. (1996). MOLMOL: a program for display and analysis of macromolecular structure. J. Mol. Graph. *14*, 51–55.

Lin, S.J., Pufahl, R., Dancis, A., O'Halloran, T.V., and Culotta, V.C. (1997). A role for the *Saccharomyces cerevisiae* ATX1 gene in copper trafficking and iron transport. J. Biol. Chem. *272*, 9215–9220.

Linder, M.C. (1991). Biochemistry of Copper (New York: Plenum Press).

Linge, J.P., Williams, M.A., Spronk, C.A.E.M., Bonvin, A.M.J.J., and Nilges, M. (2003). Refinement of protein structures in explicit solvent. Proteins *50*, 496–506.

McDonald, I.K., and Thornton, J.M. (1994). Satisfying hydrogen bonding potential in proteins. J. Mol. Biol. *238*, 777–793.

O'Halloran, T.V., and Culotta, V.C. (2000). Metallochaperones, an intracellular shuttle service for metal ions. J. Biol. Chem. *275*, 25057–25060.

Portnoy, M.E., Rosenzweig, A.C., Rae, T., Huffman, D.L., O'Halloran, T.V., and Cizewski Culotta, V. (1999). Structure-function analyses of the ATX1 metallochaperone. J. Biol. Chem. *274*, 15041–15045.

Pufahl, R.A., Singer, C.P., Peariso, K.L., Lin, S.-J., Schmidt, P.J., Fahrni, C.J., Cizewski Culotta, V., Penner-Hahn, J.E., and O'Halloran, T.V. (1997b). Metal ion chaperone function of the soluble Cu(I) receptor Atx1. Science *278*, 853–856.

Rae, T., Schmidt, P.J., Pufahl, R.A., Culotta, V.C., and O'Halloran, T.V. (1999). Undetectable intracellular free copper: the requirement of a copper chaperone for superoxide dismutase. Science *284*, 805–808.

Rosenzweig, A.C. (2001). Copper delivery by metallochaperone proteins. Acc. Chem. Res. *34*, 119–128.

Rosenzweig, A.C., Huffman, D.L., Hou, M.Y., Wernimont, A.K., Pufahl, R.A., and O'Halloran, T.V. (1999). Crystal structure of the Atx1 metallochaperone protein at 1.02 A resolution. Struct. Fold. Des. *7*, 605–617.

Sayre, L.M., Perry, G., and Smith, M.A. (1999). Redox metals and neurodegenerative disease. Curr. Opin. Chem. Biol. *3*, 220–225.

Strausak, D., Mercer, J.F., Hermann, H.D., Stremmel, W., and Multhaup, G. (2001). Copper in disorders with neurological symptoms: Alzheimer's, Menkes, and Wilson diseases. Brain Res. Bull. *55*, 175–185.

Tottey, S., Rich, P.R., Rondet, S.A.M., and Robinson, N.J. (2001). Two Menkes-type ATPases supply copper for photosynthesis in *Synechocystis* PCC 6803. J. Biol. Chem. *276*, 19999–20004.

Tottey, S., Rondet, S.A., Borrelly, G.P., Robinson, P.J., Rich, P.R., and Robinson, N.J. (2002). A copper metallochaperone for photosynthesis and respiration reveals metal-specific targets, interaction with an importer, and alternative sites for copper acquisition. J. Biol. Chem. *277*, 5490–5497.

Wallace, A.C., Laskowski, R.A., and Thornton, J.M. (1995). LIGPLOT: a program to generate schematic diagrams of protein-ligand interactions. Protein Eng. *8*, 127–134.

Wernimont, A.K., Huffman, D.L., Lamb, A.L., O'Halloran, T.V., and Rosenzweig, A.C. (2000). Structural basis for copper transfer by the metallochaperone for the Menkes/Wilson disease proteins. Nat. Struct. Biol. *7*, 766–771.

Yuan, D.S., Dancis, A., and Klausner, R.D. (1997). Restriction of copper export in Saccharomyces cerevisiae to a late Golgi or post-Golgi compartment in the secretory pathway. J. Biol. Chem. *272*, 25787–25793.

Accession Numbers

Coordinates of the HADDOCK models of the Atx1:Ccc2a complex have been deposited in the Protein Data Bank (accession codes: 1UV1, for the models calculated starting from the copper ion bound to the Atx1; and 1UV2, for the models calculated starting from the copper ion bound to the domain Ccc2a of the ATPase).